Scientific Reports

https://doi.org/10.1038/s41598-026-49731-5

Article in Press

ITO-PET electrochemical biosensor functionalized with carboxylated graphene oxide for prostate cancer biomarker detection

Received: 4 December 2025

Accepted: 16 April 2026

Published online: 09 May 2026

Cite this article as: Lim W.Y., Chin W.J., Sthaneshwar P. *et al.* ITO-PET electrochemical biosensor functionalized with carboxylated graphene oxide for prostate cancer biomarker detection. *Sci Rep* (2026). https://doi.org/10.1038/s41598-026-49731-5

Wei Yin Lim, Wee Jian Chin, Pavai Sthaneshwar, Narayanan Ramakrishnan & Choon-Hian Goh

ITO-PET Electrochemical Biosensor Functionalized with Carboxylated Graphene Oxide for Prostate Cancer Biomarker Detection

Wei Yin Lim[1,2], Wee Jian Chin[3], Pavai Sthaneshwar[4], Narayanan Ramakrishnan[1] and Choon-Hian Goh[3]*

[1] Micro and Nano Devices Laboratory, Department of Electrical and Robotics Engineering, Electrical and Computer Systems Engineering, School of Engineering, Monash University Malaysia, Bandar Sunway, 47500 Selangor, Malaysia.
[2] Department of Pharmacology, Faculty of Medicine, Universiti Malaya, 50603, Kuala Lumpur, Malaysia.
[3] Lee Kong Chian Faculty of Engineering and Science (LKCFES), Universiti Tunku Abdul Rahman, Sungai Long Campus, Jalan Sungai Long, Bandar Sungai Long, 43200 Kajang, Selangor, Malaysia.
[4]Department of Pathology, Faculty of Medicine, Universiti Malaya, 50603 Kuala Lumpur, Malaysia.

*Address correspondence to E-mail: gohch@utar.edu.my (C-H. Goh); weiyin.lim@um.edu.my (W.Y. Lim)

Abstract

Prostate cancer is considered the third most diagnosed malignancy worldwide, and early diagnosis is crucial for effective treatment and improved patient outcomes. In clinical laboratories, specific antigen detection (PSA) testing within gray zone range of 2–4 ng mL^{-1} remains challenging and typically relies on automated immunoassay analyzer, which are costly and require access to specialized laboratory facilities. Although qualitative lateral flow assays offer a low-cost alternative for use outside the laboratory, they lack the quantitative capability needed for early-stage cancer detection. In this study, we developed a portable and disposable electrochemical sensor for quantitative screening of total PSA. A carboxyl-functionalized graphene oxide (GO-COOH) layer was electrodeposited onto a flexible indium tin oxide–polyethylene terephthalate (ITO-PET) substrate to enhance conductivity and surface area, enabling sensitive biomarker detection. The biosensor exhibited a wide linear response range of 0–100 ng mL^{-1} and a low detection limit (LOD) of 1.3 ng mL^{-1}. It demonstrated high selectivity and recovery value from 85.4% –128.7%, with a relative standard deviation (RSD) below 15.5% in spiked serum samples. Overall, the developed GO-COOH@ITO-PET immunosensor successfully spans the clinically relevant cut-off levels, and

offers strong potential as a low-cost, rapid, and quantitative platform for PSA screening in point-of-care settings.

Keyword Electrochemical biosensor; Prostate-specific antigen; Carboxyl-functionalized graphene oxide; ITO–PET; Electrodeposition; Point-of-care diagnostics.

Introduction

Cancer remains a major global health challenge, causing nearly 10 million deaths in 2020 [1]. Among these, prostate cancer was the third most diagnosed malignancy, responsible for approximately 1.41 million deaths. Early diagnosis is critical for improving patient outcomes, enabling timely intervention, and reducing overall cancer-related mortality. Prostate-specific antigen (PSA) testing is widely used for early prostate cancer screening and disease monitoring. Clinically, PSA levels between 2 and 10 ng mL^{-1} are considered the diagnostic gray zone, with the lower range of 2–4 ng mL^{-1} being particularly challenging to interpret. As a result, a standard clinical cut-off of 4 ng mL^{-1} is commonly used to guide further investigation. However, conventional PSA assays such as enzyme-linked immunosorbent assay (ELISA) or chemiluminescence tests typically require centralized laboratory equipment and trained personnel, making them expensive and often inaccessible in low-resource settings. Lateral flow assays (LFAs) offer a simple point-of-care alternative, but they are generally limited to qualitative or semi-quantitative results. This drives a strong interest in developing portable, low-cost, and user-friendly diagnostic tools for quantitative PSA detection at the point of care.

Electrochemical biosensors have garnered significant attention for their potential in point-of-care diagnostics due to high sensitivity and efficiency [2-12]. However, surface functionalization strategies have commonly relied on drop-casting silanization or physical adsorption, which typically require long incubation times (several hours or often overnight) and carefully controlled conditions [13]. For example, functionalization of electrode surface often depends on the chemical activation step (e.g. ozone or alkaline treatment) to introduce hydroxyl (–OH) groups on the electrode surface for biorecognition elements (e.g., antibodies, DNA, or proteins) immobilization. These –OH groups enable subsequent silanization with organosilanes such as 3-glycidoxypropyltrimethoxysilane (3-GOPS), 3-cyanopropyltrimethoxysilane (3-CPTMS), 3-(trimethoxysilyl)propyl methacrylate (3-TMSPM), carboxyethylsilanetriol (CTES), 3-glycidoxypropyltriethoxysilane (GPTES), or (3-aminopropyl)triethoxysilane (APTES) [13-17]. Although these silane molecules form covalently bonded self-assembled monolayers that provide

reactive functional groups (epoxy, cyano, vinyl, amine, etc.) for biomolecule attachment, such processes are time-consuming and can result in surface instability. The silane layer or non-covalently bound biomolecules may detach during rigorous washing or electrochemical cycling, ultimately compromising sensor reproducibility and performance.

Recent wash-free electrochemical sensing strategies have reduced assay complexity by eliminating washing steps during signal measurement; however, most still depend on silane-based surface modification and multistep functionalization protocols [18, 19]. In contrast, silane-free surface assembly strategies based on functional nanomaterials offer a more robust and scalable alternative. Materials such as graphene oxide (GO), multiwalled carbon nanotubes (MWCNTs), and MXenes provide intrinsic surface functionalities or support polymer-assisted coupling chemistries, enabling stable covalent immobilization of biorecognition elements while improving coating reproducibility [20-23]. Notably, recent HF-free synthesis routes for MXenes have further improved their safety and scalability, enhancing their attractiveness for biosensing applications [24].

Among these materials, GO remains particularly attractive for point-of-care biosensors owing to its excellent electrical conductivity, large specific surface area, and abundance of oxygen-containing functional groups, which facilitate efficient surface modification and biomolecule immobilization [25]. Furthermore, functionalization of GO to introduce additional carboxyl (–COOH) groups enhances its chemical reactivity, enabling covalent coupling of biomolecules through EDC/NHS chemistry. This modification allows strong amide bond formation with amine-containing antibodies, resulting in dense and durable antibody immobilization while improving the biochemical stability of the sensing interface. In addition, the high surface area and conductivity of carboxyl-functionalized GO (GO-COOH) facilitate efficient antibody loading and electron transfer, thereby enhancing signal intensity and detection sensitivity compared with conventionally silanized or drop-cast electrodes. To contextualize the current progress of graphene-based electrochemical immunosensors for PSA detection, **Table 1** summarizes representative studies employing various electrode platforms. While several reported systems achieve ultralow detection limits, many rely on rigid substrates (e.g., glassy carbon or gold electrodes) that involve complex fabrication processes and limited disposability, thereby restricting their suitability for point-of-care translation. This limitation is evident in numerous high-performance graphene-based sensors reported on glassy carbon electrodes [5, 11, 12]and gold substrates [26], where excellent analytical sensitivity is achieved at the expense of fabrication cost, scalability, and single-use applicability.

Alternative electrode platforms have been explored to address these challenges. Screen-printed carbon electrodes offer improved reproducibility and moderate sensitivity[27], but their fabrication still involves specialized printing inks and equipment, resulting in relatively high per-unit cost [28]. Paper-based electrodes provide a low-cost and environmentally friendly alternative [29, 30]; however, their reproducibility and stability remain limited due to variability in paper porosity and drying effects, which collectively hinder their suitability for quantitative electrochemical assay [31]. Collectively, these trade-offs underscore the need for flexible, low-cost, and scalable electrode platforms that preserve analytical performance while enabling practical point-of-care deployment.

In contrast, indium tin oxide-coated polyethylene terephthalate (ITO-PET) substrates combine mechanical flexibility, optical transparency, and low cost, making them strong candidates for next-generation biosensing platforms. Previous studies have demonstrated the feasibility of ITO–PET-based sensors for biomarkers such as alpha-fetoprotein (AFP) [16], tumour necrosis factor α (TNF α) [14], and p21-activated kinase 2 (PAK-2) [15], as well as in an aptamer-based PSA sensor [17]. While optical and colorimetric PSA sensing strategies have also been reported, the present work focuses specifically on electrochemical detection due to its superior quantitative capability and integration potential for point-of-care applications [32].

In the present work, we introduce a graphene-based electrochemical PSA biosensor constructed via simple electrodeposition of carboxyl-functionalized graphene oxide (GO-COOH) on flexible ITO-PET electrodes, forming a uniform, adherent, and highly functionalized biointerface. This interface supports covalent immobilization of antibodies without the need for silane chemistry, enhancing mechanical and biochemical stability. Coupled with a ferrocenecarboxylic acid-labeled detection antibody and square-wave voltammetry (SWV) readout, the proposed sensor achieves sensitive and reproducible PSA detection using a compact and disposable platform—offering a novel integration of material assembly, bioconjugation, and electrochemical transduction on ITO-PET.

Table 1. Comparison of representative graphene-based electrochemical immunosensors for PSA detection, emphasizing electrode substrates, immobilization strategy, and analytical performance relevant to point-of-care testing.

Electrode substrate	Detection method	Target analyte	Immobilization strategy	Linear range (ng ml $^{-1}$)	Detection limit (ng ml $^{-1}$)	Ref.
Glassy carbon electrode	[i]DPV [ii]EIS	PSA	GO/chitosan film	[i]0.1 pg mL^{-1} – 90 ng mL^{-1} [ii]5 pg mL^{-1}	[i]10 fg mL^{-1} [ii]up to 35 ng mL^{-1}	[5]
Glassy carbon electrode	EIS	DNA sequences of prostate cancer	thioglycolic acid/gold nanoparticles/reduced GO	0.0012 pg mL^{-1} – 12,000 ng mL^{-1}	0.0004 pg mL^{-1}	[12]
Glassy carbon electrode	EIS	DNA sequences of prostate cancer	polyaniline and GO nano sheets	1.0×10^{-16}M – 1.0×10^{-8} M	3.3×10^{-17} M	[11]
Screen-printed carbon	DPV	PSA	graphene-poly(3-aminobenzoic acid) nanomaterial-conductive polymer composite	0.01 ng mL $^{-1}$ – 80 ng mL $^{-1}$	0.13 pg mL $^{-1}$	[27]
Gold substrate	DPV	PSA	reduced GO and gold nanoparticles	0.006 ng mL^{-1} – 30 ng mL^{-1}	0.003 ng mL^{-1}	[26]
Filter paper	DPV	PSA	Gold nanoparticle/reduced GO/thionine	0.05 ng mL^{-1}– 200 ng mL^{-1}	10 pg mL^{-1}	[29]
Filter paper	DPV	PSA	mesoporous carbon / carbon nanotubes /GO	10.0 ng mL^{-1}–1000 ng mL^{-1}	2.16 ng mL^{-1}	[30]

ITO-PET	SWV	PSA	Carboxyl functionalized GO	0 ng mL^{-1}– 100 ng mL^{-1}	1.3 ng mL^{-1}	This work

Experiment

Chemical and Reagents

Electrochemical studies, including cyclic voltammetry (CV) and electrochemical impedance spectroscopy (EIS), were performed using an Ossila Potentiostat (Model T2006A1, Ossila BV, The Netherlands) and portable Potentiostat/Galvanostat/Impedance Analyzer (EIS) (µStat-i 400s, Metrohm, Switzerland), respectively. Ferri/ferrocyanide solution was prepared by mixing 5 mM potassium ferrocyanide ($[Fe(CN)_6]^{4-}$) and 5 mM potassium ferricyanide ($[Fe(CN)_6]^{3-}$) in 0.1 M potassium chloride (KCl). GO powder, chloroacetic acid, sodium hydroxide (NaOH), and ferrocenecarboxylic acid. All chemicals were purchased from Sigma-Aldrich (USA). ITO film covered on polyethylene terephthalate (PET) film with a surface resistivity of 60 Ω/sq (639303-1EA) was purchased from Sigma-Aldrich. ITO-PET electrodes (15 mm x 25 mm) were used as working electrode in a three-electrode electrochemical, along with an Ag/AgCl reference electrode and a platinum counter electrode). For PSA detection, antibody 10-P20D was used as the capture antibody and 10-P20E as the detection antibody. All PSA antibodies and protein were obtained from Fitzgerald (USA). Human serum (human male AB plasma, USA origin, sterile-filtered) was purchased from Sigma-Aldrich and used for spiking and recovery studies. Clinical serum samples from prostate cancer patients were obtained from the University of Malaya Medical Center (UMMC) under approved ethical (MREC ID No : 2022418-11165). All procedures were conducted in accordance with relevant guidelines and regulations. The samples were provided in a de-identified manner and used for preliminary validation of the developed biosensor, with results compared against chemiluminescence immunoassay (CLIA) measurements performed at UMMC.

Instrument

Fourier transform infrared spectroscopy (FTIR) (Nicolet iS10 model, Thermo Fisher) with a wavelength range of 600–4000 cm^{-1}, Raman spectra characterization with a 532 nm excitation in the 3000 – 100 cm^{-1} range using Raman Spectroscopy (Renishaw InVia Raman Microscope), field emission scanning electron microscope (FESEM, Hitachi SU8010) and atomic force microscopy (AFM, Bruker Multimode 8) were used to determine the surface morphology of GO-COOH coated ITO-PET.

Preparation of Carboxyl-Modified GO as Sensing Material

The 5 mg GO was mixed with 0.12 g chloroacetic acid and 0.1 g NaOH in 10 mL of ultrapure water. The mixture underwent sonication for 3 hours. Afterward, the solution was neutralized with nitric acid (HNO_3) to pH 7. The carboxyl-modified GO was obtained and centrifuged to remove the supernatant, followed by washing with ultrapure water. The GO-COOH was dried overnight at room temperature to yield in powder form. The 1 mg mL^{-1} of GO-COOH was prepared and ready use for electrodeposition.

Electrodeposition of Carboxyl-Modified GO on ITO-PET Film

An ITO-PET film was cut in dimension of 15 mm × 25 mm and thoroughly cleaned by sequential sonication in Decon 90 detergent, ethanol, and isopropyl alcohol (IPA) for 5 minutes each to remove any residues before coating. 1 mg mL^{-1} GO-COOH solution was dispersed in water and sonicated for 10 minutes. Then, 100 µL of the GO-COOH solution was introduced into 3D printed electrochemical cell and subjected to electrodeposition on ITO-PET film within a potential range of +0.2 V to -1.5 V for 5 cycles with 20 mA current at scan rate of 50 mVs^{-1} using Ossilla Potentiostat (The Netherlands). The modification on sensor surface (with and without GO-COOH) were evaluated using a 5 mM potassium ferrocyanide/potassium ferricyanide in 0.1M KCl with a potential range of -0.4 V to 0.8 V, aligned with the Ag/AgCl reference electrode.

Preparation of Redox Probe for Assay

In this study, a redox probe utilizing ferrocenecarboxylic acid was prepared with slight modifications based on reported literature. Ferrocenecarboxylic acid served as a redox mediator and was conjugated with the detection antibody for PSA biomarker detection. Ferrocene labeling of the detection antibody was employed as a well-established electrochemical reporting strategy and is not claimed as a novel aspect of this work [33]. To prepare the probe, 5 mM ferrocenecarboxylic acid was dissolved in phosphate-buffered saline (pH 7.4) and activated with 0.2 mg of EDC and NHS. The solution was stirred for 1 hour before adding the detection anti-PSA antibody. Following the addition of all reagents, the mixture was stirred for an additional hour. The final conjugate was then

centrifuged to remove unbound ferrocenecarboxylic acid, and the redox probe was stored at 4°C until use in the assay.

Detection procedure on Carboxyl-Modified GO deposited ITO-PET

As illustrated in Fig. 1, GO-COOH electrodeposited on the ITO–PET substrate was used to facilitate capture antibody immobilization in the sandwich assay format. Following electrodeposition, the carboxyl-modified GO was chemically activated with a mixture of 20 mM EDC and 5 mM NHS for 30 minutes to enable the immobilization of the capture antibody. The COOH groups present on the ITO-PET film were activated using EDC-NHS to promote binding with the PSA capture antibody. To prevent non-specific binding, the surface was incubated with a 1% western blocking reagent for 30 minutes. The analyte was then introduced onto the surface, followed by the addition of the detection antibody conjugated with the redox probe. Surface modifications throughout the assay were characterized using cyclic voltammetry (CV) and electrochemical impedance spectroscopy (EIS) in a 5 mM potassium ferrocyanide/ferricyanide solution prepared in 0.1 M KCl, within a potential window of –0.4 V to 0.8 V vs. Ag/AgCl. Sensor fabrication steps were performed prior to analysis and are therefore not included in the reported assay time. A series of spiked PSA serum samples (0, 0.5, 1, 5, 10, 30, 50, 100ng mL^{-1}) in 1:2 diluted human serum (sterile-filtered human male AB plasma) were used contrast a matrix-matched calibration curve and to evaluate the sensor's reliability. Recovery studies were subsequently performed by spiking known amounts of PSA into diluted human serum at three concentration levels (5, 10, and 50 ng mL^{-1}). Quantitative detection of PSA was carried out using square-wave voltammetry (SWV). To evaluate the practical applicability of the sensor, a series of serum samples were obtained from prostate cancer patients at University Malaya Medical Centre (UMMC). To compensate for the substantial background current originating from the phosphate buffer (PB) electrolyte, all SWV peak current data were processed by first subtracting the blank (buffer-only) response, followed by baseline correction using Metrohm DropView software to eliminate any residual slope. This procedure ensured accurate evaluation of the ferrocenecarboxylic acid (FcCOOH) redox signals.

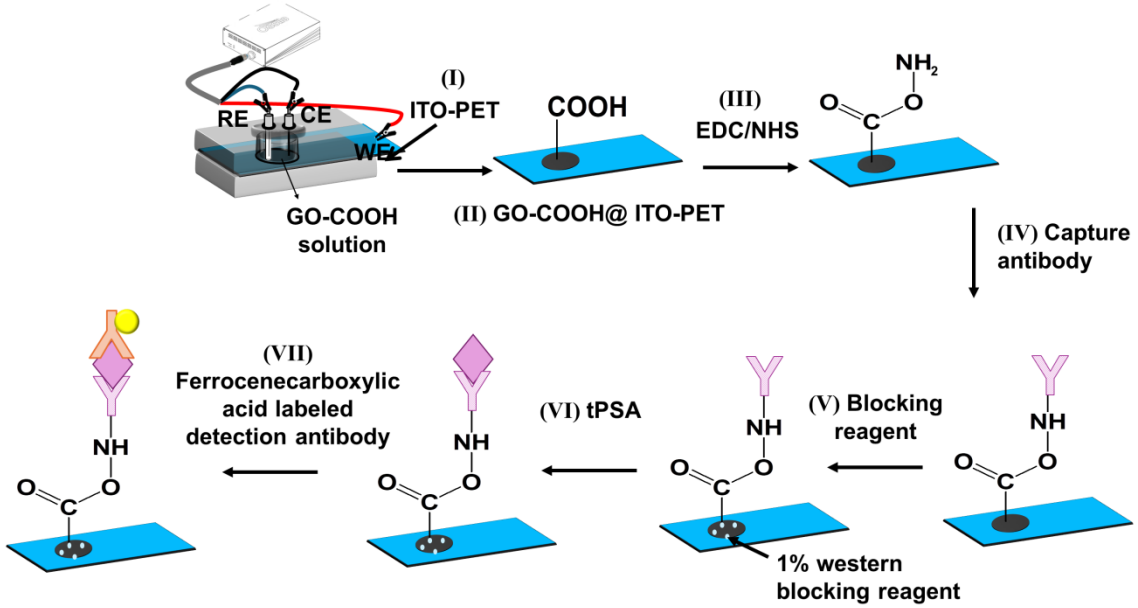

Fig. 1 Schematic illustration of the stepwise fabrication of the GO-COOH@ITO-PET electrochemical biosensor for PSA detection. Step I: bare ITO-PET electrode; Step II: electrodeposition of GO-COOH; Step III: EDC/NHS activation; Step IV: antibody immobilization; Step V: blocking of nonspecific sites; Step VI: PSA binding; Step VII: binding of FcCOOH-labeled detection antibody. Each fabrication step induces characteristic changes in the electrochemical response, as confirmed by cyclic voltammetry CV and EIS while the signal is quantified using SWV.

Result and Discussion

Characterization of GO–COOH Electrodeposited on ITO–PET

The surface morphology of the GO-COOH film electrodeposited on the ITO-PET substrate was examined using FESEM and AFM. As shown in Fig. 2a, the GO-COOH layer exhibits a dense and continuous coating across the ITO-PET surface, confirming successful electrodeposition. At higher magnification (Fig. 2b), the GO-COOH nanosheets display wrinkled and overlapping structures, characteristic of stacked GO layers. These features suggest good film uniformity and intimate contact between the GO-COOH and the underlying ITO-PET substrate, which are beneficial for efficient electron transfer during sensing. AFM images (Fig. 2c and 2d) further reveal the morphological transformation from the rough bare ITO-PET surface to a more uniform and smoother surface after GO-COOH deposition, supporting the formation of a continuous coating through the electrodeposition process.

The surface chemistry of the carboxyl-functionalized GO layer was further characterized by FTIR (Fig. 3a) and Raman spectroscopy (Fig. 3b). In the FTIR spectrum, the C=O stretching band at 1720 cm^{-1} confirms the presence of carboxyl (–COOH) functional groups, while the C-O stretching band at 1200 cm^{-1} indicates oxygenated functionalities. After EDC/NHS activation, the presence of N-H band at 3300 cm^{-1} and decrease in C=O intensity confirms the formation of amide linkages, verifying successful chemical activation of GO–COOH for biomolecule immobilization.

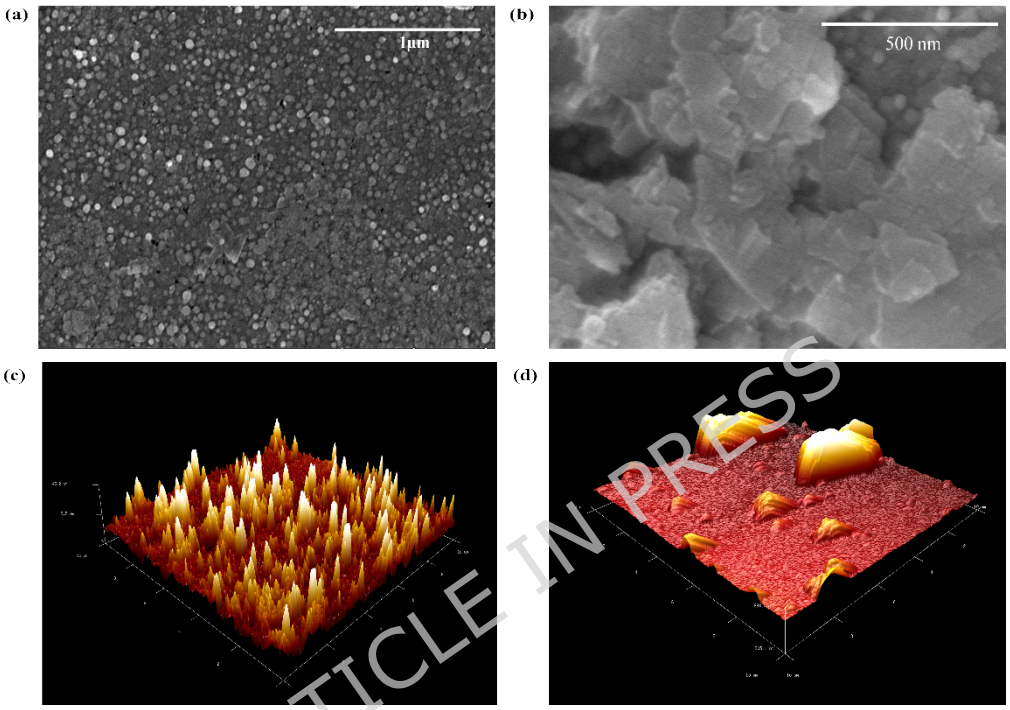

Fig. 2 Surface morphology of bare and GO-COOH–coated ITO-PET. (a) FESEM image showing dense surface coverage of GO-COOH on the ITO-PET substrate. (b) Higher-magnification FESEM revealing overlapping GO-COOH nanosheets with wrinkled structures, confirming successful electrophoretic deposition. (c) AFM image of bare ITO-PET. (d) AFM image of GO-COOH–coated ITO-PET showing a more uniform surface with fewer high peaks, indicating the formation of a continuous film.

The Raman spectrum revealed the characteristic D and G bands of GO at 1361cm^{-1} and 1583 cm^{-1}, respectively. The D band corresponds to structural disorder, while the G band reflect the bond stretching of sp^2 carbon atoms [34]. The I_D/I_G ratio represents the intensity of the D band to the G band, reflects the degree of disorder or defects within the GO structure. A higher I_D/I_G ratio indicates more defects, whereas a lower ratio indicates a more ordered with fewer defects, signifying higher-quality graphene structure [35]. In this study, the GO-COOH exhibited a moderate level of defects, as indicated by an I_D/I_G ratio of 0.63. This reflects

successful carboxyl functionalization that increases surface defects while preserving the sp^2 carbon backbone. Notably, the 2D band observed around 2739 cm^{-1}, further confirms the partial retention of graphitic ordering despite oxidation and surface modification.

X-ray photoelectron spectroscopy (XPS) (Fig. 3c) confirmed the successful carboxyl functionalization of GO with carboxylic acid groups following treatment with chloroacetic acid and NaOH. The survey spectrum revealed dominant C1s and O1s peaks, with minor In and Sn signals originating from the ITO substrate. It also showed a balanced carbon-to-oxygen (C/O) ratio of approximately 1.1, reflecting an optimal degree of oxidation for carboxyl functionalization. Trace N and Ca signals (< 1%) were detected, which likely originated from residual nitrate species introduced during pH adjustment with nitric acid and minor Ca^{2+} contamination from rinsing. These signals are negligible and do not contribute to the GO–COOH chemical structure.

The high-resolution C1s spectrum of GO–COOH (Fig. 3d(i)) reveals multiple components indicative of various carbon environments. The main peak at 284.8 eV corresponds to sp^2-hybridized C=C bonds of the graphene backbone, while the shoulder at 284.85 eV is attributed to sp^3-hybridized C–C carbon arising from structural defects or edge carbon atoms. Peaks at 286.3 eV and 287.3 eV are assigned to C–O and C=O functionalities, respectively, confirming the presence of oxygen-containing groups introduced through oxidation. The small feature around 289.0 eV represents a π–π* satellite, characteristic of delocalized π-electron systems in aromatic structures. These results confirm the partial oxidation of GO and the successful introduction of carboxyl groups essential for EDC/NHS-mediated antibody immobilization. The high-resolution O1s spectrum of GO–COOH (Fig. 3d(ii)) was deconvoluted into three primary components. The peak at 531.4 eV corresponds to C=O groups, including carbonyl and carboxylic acid functionalities, indicating successful oxidation of the carbon framework. A second peak positioned at 532.2 eV is attributed to C–O species such as hydroxyl and epoxy groups, which are characteristic of GO sheets. The small shoulder observed at 533.9 eV may be associated with additional C–O moieties or weakly adsorbed oxygen species on the surface. These results confirm the presence of abundant oxygen-containing functional groups, particularly carboxyl and hydroxyl groups, which are essential for subsequent covalent antibody immobilization via EDC/NHS coupling.

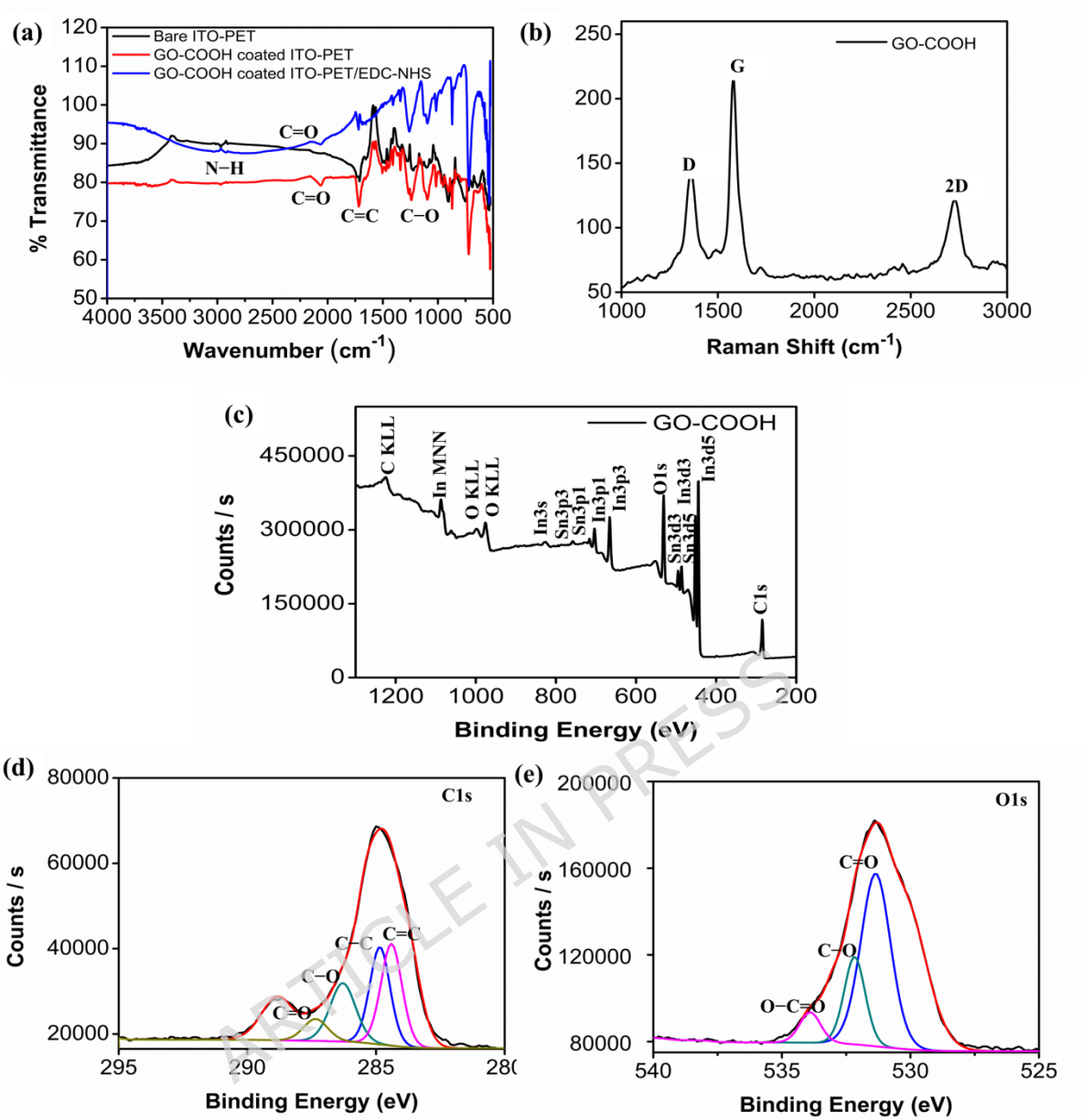

Fig. 3 (a) FTIR on surface modification on ITO-PET film with bare, GO-COOH coated and GO-COOH with EDC/NHS, (b) Raman spectra and (c) XPS survey scan of GO-COOH coated on ITO-PET and elemental profile: (i) C1s and (ii) O1s

Electrochemical Characterization of Stepwise Modification

To optimize coating thickness, the influence of the number of deposition cycles on the electrochemical behavior of GO-COOH@ITO-PET was examined (Fig. 4a). At a scan rate of 50 mV s^{-1}, the 5-cycle coating exhibited the highest conductivity compared with uncoated and more heavily coated electrodes. Increasing the cycle number beyond 10 caused

a rightward shift and decreased peak currents in the CV profiles, indicating thicker films that hinder electron transfer. Thus, five deposition cycles were selected as the optimal condition. During the electrodeposition process, the CV curves (Fig. 4b) show a progressive current increase across successive scans up to five cycles, indicating successful electrodeposition of GO-COOH. The cathodic peak near –1.3 V corresponds to GO partial reduction, which enhances film adhesion and conductivity. The stabilization of current peaks across cycles confirms uniform and reproducible film formation.

Cyclic voltammetry was further employed to monitor the redox response during each modification step using the ferri/ferrocyanide ($[Fe(CN)_6]^{3-/4-}$) redox probe (Fig. 4c). The bare ITO-PET electrode (Stage I) exhibited relatively low redox peak currents, reflecting its limited electrochemical activity. After coating with GO-COOH (Stage II), the peak currents increased due to the enhanced electron transfer kinetics provided by the high surface area and conductivity of the GO layer. Following EDC-NHS activation (Stage III), a slight decrease in peak current was observed, likely due to the formation of less conductive NHS ester intermediates. The immobilization of the capture antibody (Stage IV) and blocking agent (Stage V) further suppressed the current, as these insulating biomolecular layers hindered access of the redox probe to the electrode surface. Upon the addition of the target analyte (Stage VI), the redox peaks became more flattened, consistent with additional surface coverage and increased electron transfer resistance. Finally, the addition of the ferrocenecarboxylic acid-conjugated detection antibody (Stage VII) resulted in further peak suppression, confirming the completion of the sandwich immunoassay and successful stepwise surface modification.

Electrochemical impedance spectroscopy (EIS) provided complementary insight into interfacial changes. The Nyquist plots (Fig. 4d) were fitted using an equivalent R(C(RW)) circuit, where R_s denotes solution resistance, C is double-layer capacitance, Rct is charge-transfer resistance, and W is Warburg impedance. The decrease in R_{ct} at Stage II, confirms enhanced electron transfer through the GO-COOH layer. From Stage III to Stage VI, R_{ct} increased progressively, indicating the sequential formation of insulating biomolecular layers on the electrode. At Stage VII, the introduction of the detection antibody conjugates further increased R_{ct}, likely due to specific target–antibody interactions that reduced electron transfer at the interface. These EIS results are consistent with the CV data and validate the successful layer-by-layer biosensor assembly.

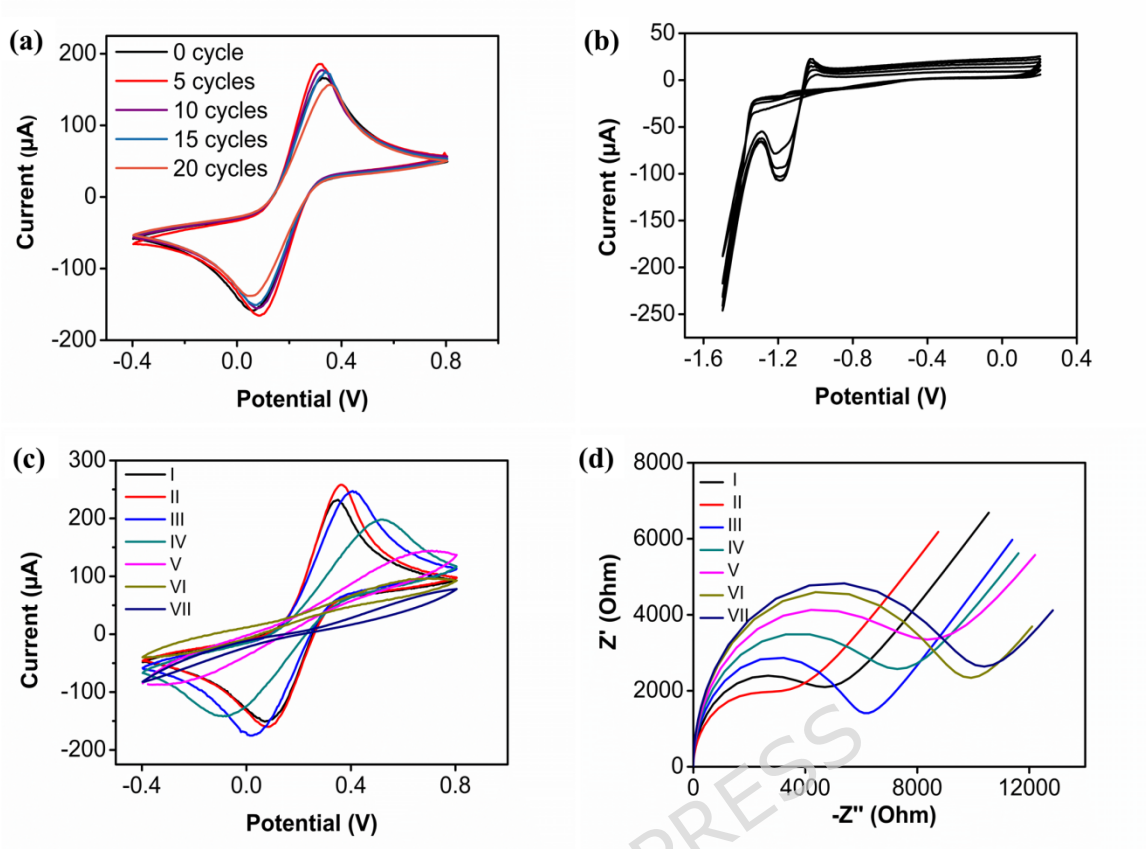

Fig. 4 (a) Electrodeposition was performed using different cycle numbers (0, 5, 10, 15, 20) at a scan rate of 50 $mVs^{-1}$with current range of 20 mA. (b) The EPD process for 5 cycles with GO-COOH on ITO-PET at potential of +0.2 V to -1.5 V(c) CV curve and (d) EIS Nyquist plot of modification stage of bare and GO-COOH coated ITO-PET. CV curves at each modification stage on ITO-PET: (I) Bare ITO-PET, (II) GO-COOH coated, (III) EDC-NHS activation, (IV) Capture antibody addition, (V) blocking reagent addition, (VI) target analyte addition, (VII) ferrocenecarboxylic acid-conjugated detection antibody addition

Calibration Curve and Sensor Performance Evaluation

For quantitative analysis, a calibration curve was obtained from square-wave voltammetry (SWV) by monitoring the redox peak current of surface-bound ferrocenecarboxylic acid (FcCOOH). Total PSA concentrations in diluted human serum ranging from 0 to 100 ng mL^{-1} were tested using the GO-COOH coated ITO-PET sensor. The SWV peak current increased proportionally with rising PSA levels, reflecting the formation of the antibody–antigen–FcCOOH-labeled sandwich complex on the electrode surface and the corresponding accumulation of redox-active Fc tags. To improve peak resolution, baseline correction was applied to the SWV traces to eliminate background contributions from PB buffer and highlight

the FcCOOH redox peak at approximately 0.34 V. The use of an FcCOOH-labeled detection antibody introduces additional conjugation steps compared to label-free electrochemical sensing approaches. Label-free methods often rely on impedance-based measurements, which can be more susceptible to nonspecific adsorption and matrix effects in complex biological samples. Enzyme-based amplification strategies, while highly sensitive, may suffer from enzyme instability, additional reagent requirements, and longer assay times. In contrast, the FcCOOH labeling strategy employed here provides a stable and well-defined redox signal without the need for enzymatic substrates, enabling robust and quantitative detection with a simplified electrochemical readout.

As shown in Fig. 5a, the sensor exhibited a well-defined concentration-dependent response. The corresponding calibration curve (Fig. 5b) demonstrated strong linearity over the 0–100 ng mL^{-1} range, with a correlation coefficient (R^2) of 0.994. Based on the 3σ/slope method, the calculated limit of detection (LOD) was approximately 1.3 ng mL^{-1}. This value lies within the clinically relevant range for early detection and monitoring of prostate cancer. The broad dynamic range, strong linearity, and low LOD highlight the potential of this flexible, Fc-tagged electrochemical immunosensor for point-of-care PSA diagnostics. The sensitivity of the biosensor was determined from the slope of the linear calibration curve and was calculated to be 0.012 µA (ng mL^{-1}) $^{-1}$.

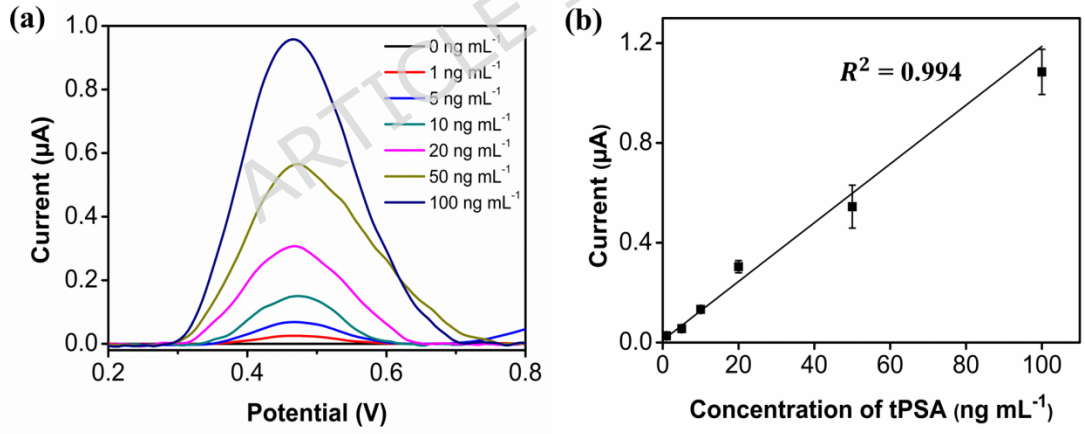

Fig. 5 (a) SWV responses of the GO-COOH@ITO-PET sensor toward PSA concentrations from 0 to 100 ng mL^{-1}, and (b) the corresponding calibration curve (SWV peak current vs. PSA).

Analytical performance for PSA detection

As shown in Fig. 6a, the charge transfer resistance (Rct) values decreased consistently after GO-COOH coating compared to the bare ITO-PET electrode across five replicates, with an RSD of approximately 10.3%.

This reduction confirms that the GO-COOH modification enhances the electrode's conductivity and facilitates faster electron transfer. The reproducibility of the sensor was evaluated by measuring the response of multiple independently fabricated GO-COOH@ITO-PET electrodes, yielding an RSD of 15.5%, demonstrating good sensor-to-sensor reproducibility and fabrication consistency (Fig. 6b). Together, these results highlight the reproducibility of the electrophoretically deposited GO-COOH coating and the consistent electrochemical response of the ITO-PET biosensor for PSA detection, supporting its potential as a point-of-care diagnostic platform. The selectivity of the GO-COOH@ITO-PET biosensor was evaluated using various non-target proteins, including BSA, IgG, and cardiac troponin T (cTnT) (Fig. 6c). The biosensor exhibited the highest current response toward PSA compared to other tested proteins, confirming its excellent selectivity. This high specificity arises from the strong antibody–antigen binding affinity and the low level of nonspecific adsorption on the GO-COOH–modified surface.

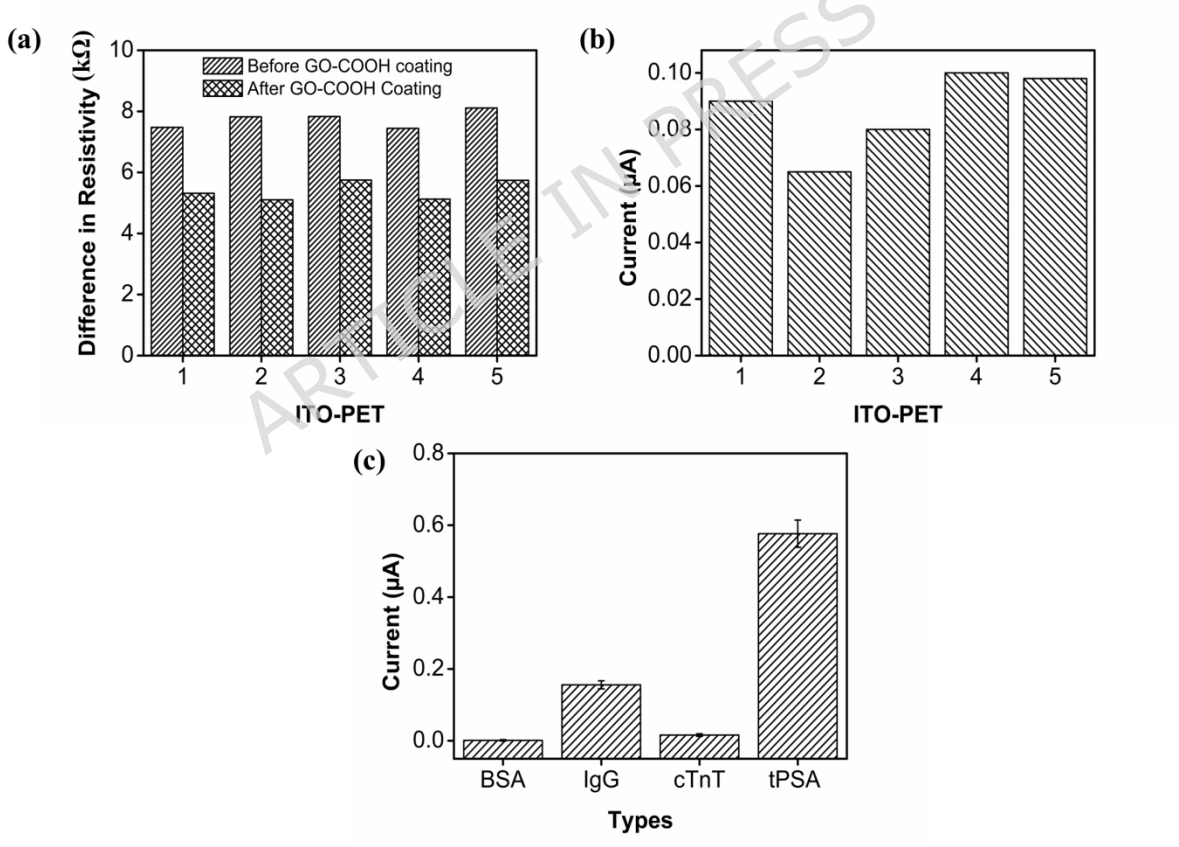

Fig. 6 (a) Comparison of charge transfer resistance (Rct) before and after GO-COOH coating on ITO-PET electrodes (n = 5). (b) Reproducibility of the GO-COOH@ITO-PET biosensor evaluated at 10 ng mL^{-1} PSA (n = 5) (c) Selectivity of the biosensor tested at 50 ng mL^{-1} PSA against potential interfering proteins (BSA, IgG, and cTnT, each at 50 ng mL^{-1}).

Application in human serum samples

To evaluate the practical applicability of the GO-COOH coated ITO-PET immunosensor, recovery studies were conducted using spiked human serum samples. Known amounts of PSA were added at three concentration levels: 5, 10, and 50 ng mL^{-1} into diluted human serum (1:2 ratio) and the measured concentrations were determined using a matrix-matched calibration curve constructed in diluted human serum (Fig. 5b). The recovery percentage was calculated as follows:

$$\text{Recovery (\%)} = \frac{\text{Measured Concentration}}{\text{Spiked Concentration}} \times 100\% \quad (1)$$

As summarized in **Table 2**, the recovery values obtained from spiked human serum samples ranged from 85.4% to 128.7%. The elevated recovery observed at the lowest concentration level (5 ng mL^{-1}) is primarily attributed to matrix effects associated with complex biological samples, as well as the proximity of this concentration to the sensor's LOD. At concentrations near the LOD, small absolute variations in electrochemical signal can result in disproportionately larger percentage deviations, which is a commonly reported phenomenon in electrochemical biosensing systems [26]. Importantly, this deviation was not consistently observed across all concentration levels, as recovery values at higher concentrations (10 and 50 ng mL^{-1}) remained closer to the acceptable range, indicating stable sensor performance under typical analytical conditions [36]. Despite the observed variation in recovery, the RSD values remained below 15.5% across all measurements, demonstrating good repeatability and consistent sensor response. This indicates that the variation is more likely due to systematic matrix-related effects rather than random measurement instability.

Overall, these findings support the feasibility of the proposed sensor for PSA detection in complex biological matrices. Nevertheless, further optimization such as improved surface blocking strategies and refined matrix-matched calibration is needed to enhance analytical accuracy in future studies.

Table 2. Recovery analysis of PSA in spiked human serum samples at different concentrations (n = 3).

Sample	Spiked Concentration (ng mL^{-1})	Measured Concentration (ng mL^{-1})	Average Recovery (%)	RSD (%)

Spiked Serum	5	6.1 6.8 6.4	128.7	5.46
	10	9.1 12.1 9.7	103.0	15.41
	50	43.1 40.8 44.2	85.4	4.06

Clinical Validation

The clinical applicability of the developed GO–COOH@ITO–PET biosensor was further assessed using serum samples obtained from prostate cancer patients, with the results validated by standard laboratory CLIA method performed at the UMMC (**Table 3**). The proposed sensor showed good concordance with the CLIA method, particularly for samples with PSA concentrations above 3 ng mL^{-1}, where deviations were within 10–20%. Slightly higher readings at low PSA levels (< 1 ng mL^{-1}) may be attributed to matrix effects and proximity to the sensor's LOD (1.3 ng mL^{-1}). These findings validate the accuracy and reliability of the proposed electrochemical platform for quantitative PSA detection in clinical serum samples. Bland–Altman analysis (Fig. 7) also showed a mean bias (dotted line) was close to zero, indicating no significant systematic error between the two methods. All measurements fell within the 95% limits of agreement (dashed lines), confirming satisfactory concordance. Slight deviations observed at higher PSA concentrations may be attributed to partial signal saturation, whereas smaller variations at low concentrations (< 3 ng mL^{-1}) reflect the influence of matrix effects near the sensor's LOD. Overall, the narrow bias range demonstrates that the biosensor provides results comparable to the CLIA method for clinical PSA quantification. Although the number of clinical serum samples analyzed in this study is limited, the results serve as a preliminary clinical validation, demonstrating the feasibility and translational potential of the GO–COOH@ITO–PET biosensor for PSA quantification, with larger cohort studies warranted in future work.

Table 3. Comparison of PSA concentrations in clinical serum samples measured by the proposed sensor and by the CLIA method from UMMC.

Serum sample	CLIA reference (ng mL^{-1})	Proposed sensor (n=3) (ng mL^{-1})	Mean ± SD (ng mL^{-1})
1	0.53	1.5/2.3/2.7	2.2 ± 0.6
2	1.28	1.1/2.1/1.2	1.5 ± 0.5
3	3.75	3.2/3.9/2.7	3.3 ± 0.6
4	7.58	9.8/8.5/9.4	9.2 ± 0.7
5	20.99	23.8/17.9/14.7	18.8 ± 4.6
6	47.41	49.3/38.6/34.5	40.8 ± 7.6

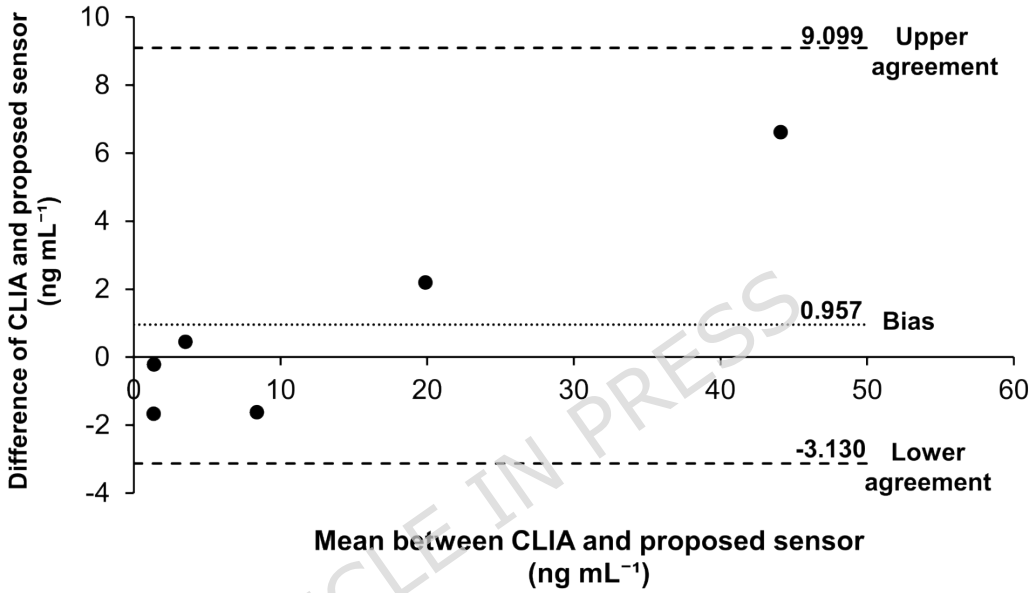

Fig. 7. Bland–Altman analysis illustrating the agreement between PSA concentrations measured by the standard CLIA method and the GO–COOH@ITO–PET biosensor (n = 6).

Conclusion

In this study, we developed a portable, disposable electrochemical biosensor for the rapid and sensitive detection of PSA in human serum. GO-COOH was electrodeposited onto ITO-PET substrates, enabling a uniform and reproducible coating for stable biosensor fabrication. The sensor exhibited a wide dynamic range (0–100 ng mL^{-1}) and a low LOD of 1.3 ng mL^{-1}, demonstrating its capability for PSA quantification across clinically relevant concentrations. Recovery studies in spiked human serum samples obtained values of 85.4% to 128.7%, reflecting the influence of matrix effects and signal variability at low concentrations, while maintaining acceptable repeatability. The use of FcCOOH as a redox label enabled clear, quantifiable electrochemical signals even after

antibody conjugation and biolayer assembly. Importantly, the proposed biosensor spans the standard clinical cut-off of 4 ng mL^{-1} for prostate cancer and exhibits analytical sensitivity suitable for detecting PSA concentrations near the gray-zone range (2–4 ng mL^{-1}), supported by its low limit of detection 1.3 ng mL^{-1}. With a total assay time of approximately 20–25 minutes after sensor preparation, the platform shows strong potential for point-of-care applications. Clinical feasibility was further demonstrated through validation using real human serum samples, which showed good agreement with the standard CLIA method. However, this validation was conducted using a limited number of samples and should be considered as a proof-of-concept demonstration of analytical feasibility. Future studies will focus on statistically powered validation in larger clinical cohort, as well as further optimization, to minimize matrix effects and improve analytical accuracy. In addition, batch-to-batch reproducibility, same-sensor repeatability, and long-term storage stability, which were not systematically evaluated in the present study, will be addressed in future investigations to support scalable fabrication and practical deployment of the proposed biosensing platform.

Author contributions

Wei Yin Lim: Conceptualization, Data curation, Writing – original draft, Investigation; **Choon-Hian Goh:** Methodology, Project administration, Writing – review & editing; **Wee Jian Chin:** Methodology, Writing – review & editing; **Pavai Sthaneshwar:** Resources, Data curation; **Narayanan Ramakrishnan**: Supervision, Project administration, Writing – review & editing.

Funding

This study was funded by a research grant from Majlis Kanser Nasional (MAKNA) (MCRCF-2021-002).

Data availability

The datasets generated and analyzed during the current study are not publicly available due to ethical restrictions associated with human serum samples but are available from the corresponding author upon reasonable request.

Ethical approval

This study received ethical approval with a waiver of informed consent from the Medical Research Ethics Committee, University Malaya Medical Centre (MREC ID No.: 2022418-11165), as it used existing stored blood samples without access to any identifiable participant information. All procedures were conducted in accordance with relevant guidelines and regulations.

Clinical trial registration: Not applicable.

Clinical trial number: Not applicable.

Declarations

Competing interests

The authors declare no competing interests.

Reference

[1] MB Culp, I Soerjomataram, JA Efstathiou, F Bray, A Jemal (2020) Recent global patterns in prostate cancer incidence and mortality rates. Eur. Urol. 77: 38. https://doi.org/10.1016/j.eururo.2019.08.005

[2] Z Akbari jonous, JS Shayeh, F Yazdian, A Yadegari, M Hashemi, M Omidi (2019) An electrochemical biosensor for prostate cancer biomarker detection using graphene oxide–gold nanostructures. Eng. Life Sci. 19: 206. https://doi.org/10.1002/elsc.201800093

[3] Y Fang, Y Li, M Zhang, B Cui, Q Hu, L Wang (2019) A novel electrochemical strategy based on porous 3D graphene-starch architecture and silver deposition for ultrasensitive detection of neuron-specific enolase. Analyst 144: 2186. https://doi.org/10.1039/C8AN02230E

[4] S Hassani, AS Maghsoudi, MR Akmalet al (2020) A sensitive aptamer-based biosensor for electrochemical quantification of PSA as a specific diagnostic marker of prostate cancer. J. Pharm. Pharm. Sci. 23: 243. https://doi.org/10.18433/jpps31171

[5] B Kavosi, A Salimi, R Hallaj, F Moradi (2015) Ultrasensitive electrochemical immunosensor for PSA biomarker detection in prostate cancer cells using gold nanoparticles/PAMAM dendrimer loaded with enzyme linked aptamer as integrated triple signal amplification strategy. Biosens. Bioelectron. 74: 915. https://doi.org/10.1016/j.bios.2015.07.064

[6] L-H Pan, S-H Kuo, T-Y Lin, C-W Lin, P-Y Fang, H-W Yang (2017) An electrochemical biosensor to simultaneously detect VEGF and PSA for early prostate cancer diagnosis based on graphene oxide/ssDNA/PLLA nanoparticles. Biosens. Bioelectron. 89: 598. https://doi.org/10.1016/j.bios.2016.01.077

[7] P Sarkar, D Ghosh, D Bhattacharyay, SeJ Setford, AePeF Turner (2008) Electrochemical immunoassay for free prostate specific antigen (f-PSA) using magnetic beads. Electroanalysis 20: 1414. https://doi.org/10.1002/elan.200804194

[8] JC Soares, AC Soares, VC Rodrigueset al (2019) Detection of the prostate cancer biomarker PCA3 with electrochemical and impedance-based biosensors. ACS Appl. Mater. Interfaces 11: 46645. https://doi.org/10.1021/acsami.9b19180
[9] L Suresh, JS Bondili, PK Brahman (2020) Fabrication of immunosensor based on polyaniline, fullerene-C60 and palladium nanoparticles nanocomposite: an electrochemical detection tool for prostate cancer. Electroanalysis 32: 1439. https://doi.org/10.1002/elan.201900659
[10] L Suresh, PK Brahman, KR Reddy, B JS (2018) Development of an electrochemical immunosensor based on gold nanoparticles incorporated chitosan biopolymer nanocomposite film for the detection of prostate cancer using PSA as biomarker. Enzyme Microb. Technol. 112: 43. https://doi.org/10.1016/j.enzmictec.2017.10.009
[11] MD Tezerjani, A Benvidi, M Rezaeinasabet al (2016) An impedimeric biosensor based on a composite of graphene nanosheets and polyaniline as a suitable platform for prostate cancer sensing. Anal. Methods 8: 7507. https://doi.org/10.1039/C6AY01524G
[12] MD Tezerjani, A Benvidi, S Jahanbani, SM Moshtaghioun, M Mazloum-Ardakani (2016) A comparative investigation for prostate cancer detection using two electrochemical biosensors based on various nanomaterials and the linker of thioglycolic acid. J. Electroanal. Chem. 778: 23. https://doi.org/10.1016/j.jelechem.2016.08.009
[13] B Vural, M ÇaliŞkan, MK SezgİntÜrk (2020) Development of a biosensor platform based on ITO sheets modified with 3-glycidoxypropyltrimethoxysilane for early detection of TRAP1. Turk. J. Chem. 44: 461. https://doi.org/10.3906/kim-1909-53
[14] E Burcu Aydın (2020) A label-free and sensitive impedimetric immunosensor for TNF α biomarker detection based on epoxysilane-modified disposable ITO-PET electrode. Int. J. Environ. Anal. Chem. 100: 363. https://doi.org/10.1080/03067319.2019.1679807
[15] B Demirbakan, MK Sezgintürk (2019) A novel electrochemical immunosensor based on disposable ITO-PET electrodes for sensitive detection of PAK 2 antigen. J. Electroanal. Chem. 848: 113304. https://doi.org/10.1016/j.jelechem.2019.113304
[16] B Özcan, H Özay, Ö Özay, MK Sezgintürk (2024) Early detection of the ovarian cancer with a label-free and disposable ITO-PET based immunosensor platform. Microchem. J. 205: 111340. https://doi.org/10.1016/j.microc.2024.111340
[17] C Özyurt, İ Uludağ, MK Sezgintürk (2023) An ultrasensitive and disposable electrochemical aptasensor for prostate-specific antigen (PSA) detection in real serum samples. Anal. Bioanal. Chem. 415: 1123. https://doi.org/10.1007/s00216-022-04309-8
[18] G Dutta, S Kim, S Park, H Yang (2014) Washing-free heterogeneous immunosensor using proximity-dependent electron mediation between an enzyme label and an electrode. Anal. Chem. 86: 4589. https://doi.org/10.1021/ac5006487
[19] G Dutta, S Park, A Singh, J Seo, S Kim, H Yang (2015) Low-interference washing-free electrochemical immunosensor using glycerol-

3-phosphate dehydrogenase as an enzyme label. Anal. Chem. 87: 3574. http://dx.doi.org/10.1021/ac504485a
[20] T Sarkar, N Dutta, G Dutta (2023) A new biosensing platform based on L-cysteine-capped Fe3O4 nanoparticles embedded in chitosan-MWCNT matrix: electrochemical kinetic and sensing studies. Biosens. Bioelectron.:X 15: 100412. https://doi.org/10.1016/j.biosx.2023.100412
[21] M Safarpoor, A Asfaram, M Ghaedi, R Dinarvand (2025) Ultrasensitive electrochemical biosensor based on MXene quantum dots for prostate cancer biomarker detection. Sci. Rep. 15: 42722. https://doi.org/10.1038/s41598-025-26754-y
[22] L Lorencova, P Kasak, N Kosutovaet al (2024) MXene-based electrochemical devices applied for healthcare applications. Microchimica Acta 191: 88. https://doi.org/10.1007/s00604-023-06163-6
[23] L Jia, Z Lei, N Zareet al (2025) Ti3C2 MXene-enhanced Electrochemical Biosensors for Prostate-Specific Antigen (PSA) Detection in Prostate Cancer. J. Nanostruct. Chem. 15: 1. https://doi.org/10.57647/jnsc.2025.1501.02
[24] K Mahabari, RD Mohili, M Patel, AH Jadhav, K Lee, NK Chaudhari (2024) HF-free microwave-assisted synthesis of MXene as an electrocatalyst for hydrogen evolution in alkaline media. Nanoscale Adv. 6: 5388. https://doi.org/10.1039/D4NA00250D
[25] S Shahriari, M Sastry, S Panjikar, R Singh Raman (2021) Graphene and Graphene Oxide as a Support for Biomolecules in the Development of Biosensors. Nanotechnol., Sci. Appl.: 197. https://doi.org/10.2147/nsa.s334487
[26] S Barman, M Hossain, JY Park (2017) Gold nanoparticles assembled chemically functionalized reduced graphene oxide supported electrochemical immunosensor for ultra-sensitive prostate cancer detection. J. Electrochem. Soc. 164: B234. https://doi.org/10.1007/s11705-019-1846-8
[27] C Pothipor, N Wiriyakun, T Putninet al (2019) Highly sensitive biosensor based on graphene–poly (3-aminobenzoic acid) modified electrodes and porous-hollowed-silver-gold nanoparticle labelling for prostate cancer detection. Sens. Actuators, B 296: 126657. https://doi.org/10.1016/j.snb.2019.126657
[28] G Paimard, E Ghasali, M Baeza (2023) Screen-printed electrodes: Fabrication, modification, and biosensing applications. Chemosensors 11: 113. https://doi.org/10.3390/chemosensors11020113
[29] B Wei, K Mao, N Liu, M Zhang, Z Yang (2018) Graphene nanocomposites modified electrochemical aptamer sensor for rapid and highly sensitive detection of prostate specific antigen. Biosens. Bioelectron. 121: 41. https://doi.org/10.1016/j.bios.2018.08.067
[30] J Soongsong, M Arivazhagan, P Banet, P-H Aubert, J Jakmunee (2025) Microfluidic paper-based electrochemical immunosensor for the detection of prostate-specific antigen (PSA) based on modified flexible screen-printed carbon electrodes. ACS Omega 10: 31009. https://doi.org/10.1021/acsomega.5c04238

[31] S Malik, J Singh, K Sainiet al (2024) Paper based sensors: affordable, versatile, and emerging analyte detection platforms. Anal. Methods 16: 2777. https://doi.org/10.1039/D3AY02258G
[32] WY Lim, WJ Chin, G Packirisamy, P Sthaneshwar, N Ramakrishnan, C-H Goh (2026) Advancing Prostate Cancer Diagnostics: The Potential of Paper-Based Biosensors for Point-of-Care Testing. Clin. Chim. Acta: 120872. https://doi.org/10.1016/j.cca.2026.120872
[33] M Kondzior, I Grabowska (2020) Antibody-electroactive probe conjugates based electrochemical immunosensors. Sensors 20: 2014. https://doi.org/10.3390/s20072014
[34] A Munir, Tu Haq, A Qurashi, HU Rehman, A Ul-Hamid, I Hussain (2018) Ultrasmall Ni/NiO nanoclusters on thiol-functionalized and-exfoliated graphene oxide nanosheets for durable oxygen evolution reaction. ACS Appl. Energy Mater. 2: 363. https://doi.org/10.1021/acsaem.8b01375
[35] W Wu, Z Liu, LA Jaureguiet al (2010) Wafer-scale synthesis of graphene by chemical vapor deposition and its application in hydrogen sensing. Sens. Actuators, B 150: 296. https://doi.org/10.1016/j.snb.2010.06.070
[36] EMA (EMA). (2022) ICH guideline M10 on bioanalytical method validation: Step 5.Available at: https://www.ema.europa.eu/en/documents/scientific-guideline/ich-guideline-m10-bioanalytical-method-validation-step-5_en.pdf. (accessed 5 November 2025).

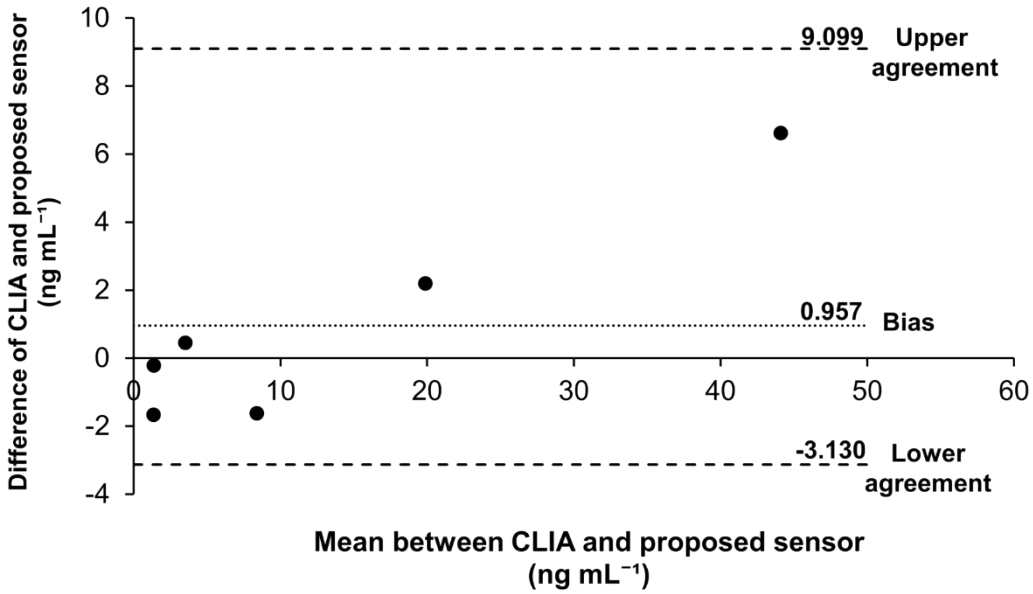

Fig. 7. Bland–Altman analysis illustrating the agreement between PSA concentrations measured by the standard CLIA method and the GO–COOH@ITO–PET biosensor (n = 6).

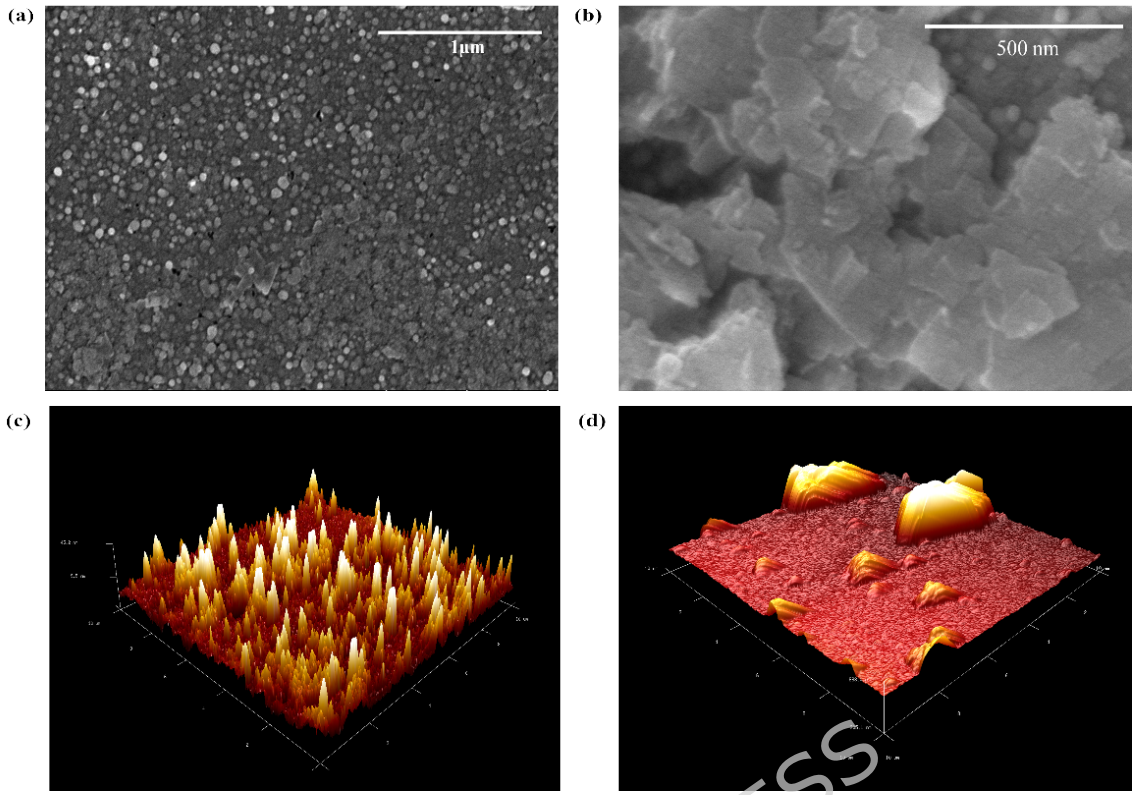

Fig. 2 Surface morphology of bare and GO-COOH–coated ITO-PET. (a) FESEM image showing dense surface coverage of GO-COOH on the ITO-PET substrate. (b) Higher-magnification FESEM revealing overlapping GO-COOH nanosheets with wrinkled structures, confirming successful electrophoretic deposition. (c) AFM image of bare ITO-PET. (d) AFM image of GO-COOH–coated ITO-PET showing a more uniform surface with fewer high peaks, indicating the formation of a continuous film.

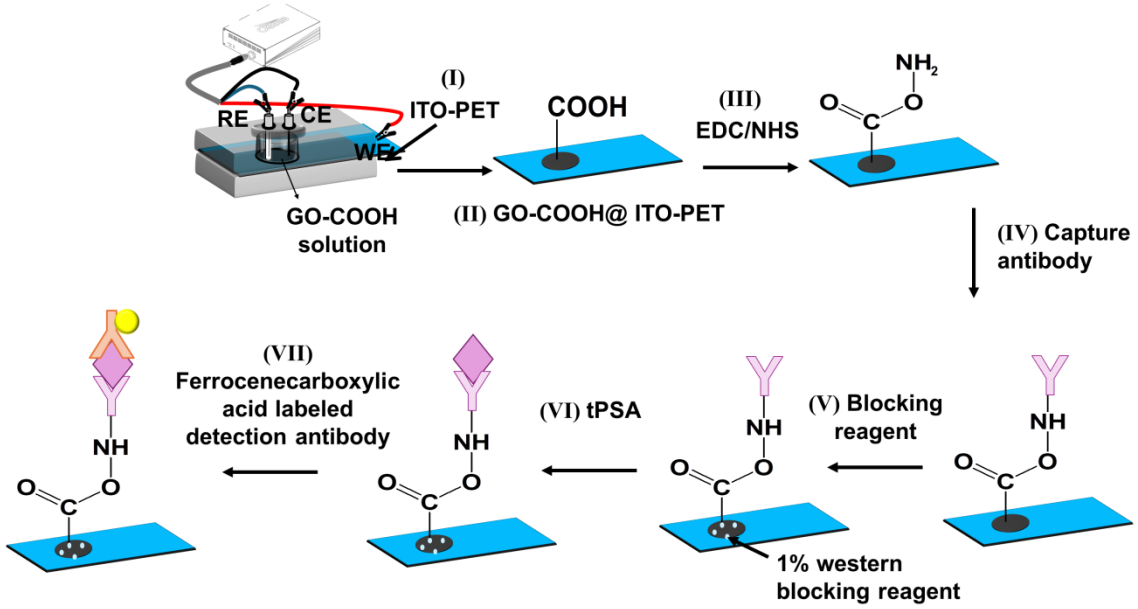

Fig. 1 Schematic illustration of the stepwise fabrication of the GO-COOH@ITO-PET electrochemical biosensor for PSA detection. Step I: bare ITO-PET electrode; Step II: electrodeposition of GO-COOH; Step III: EDC/NHS activation; Step IV: antibody immobilization; Step V: blocking of nonspecific sites; Step VI: PSA binding; Step VII: binding of FcCOOH-labeled detection antibody. Each fabrication step induces characteristic changes in the electrochemical response, as confirmed by cyclic voltammetry CV and EIS while the signal is quantified using SWV.

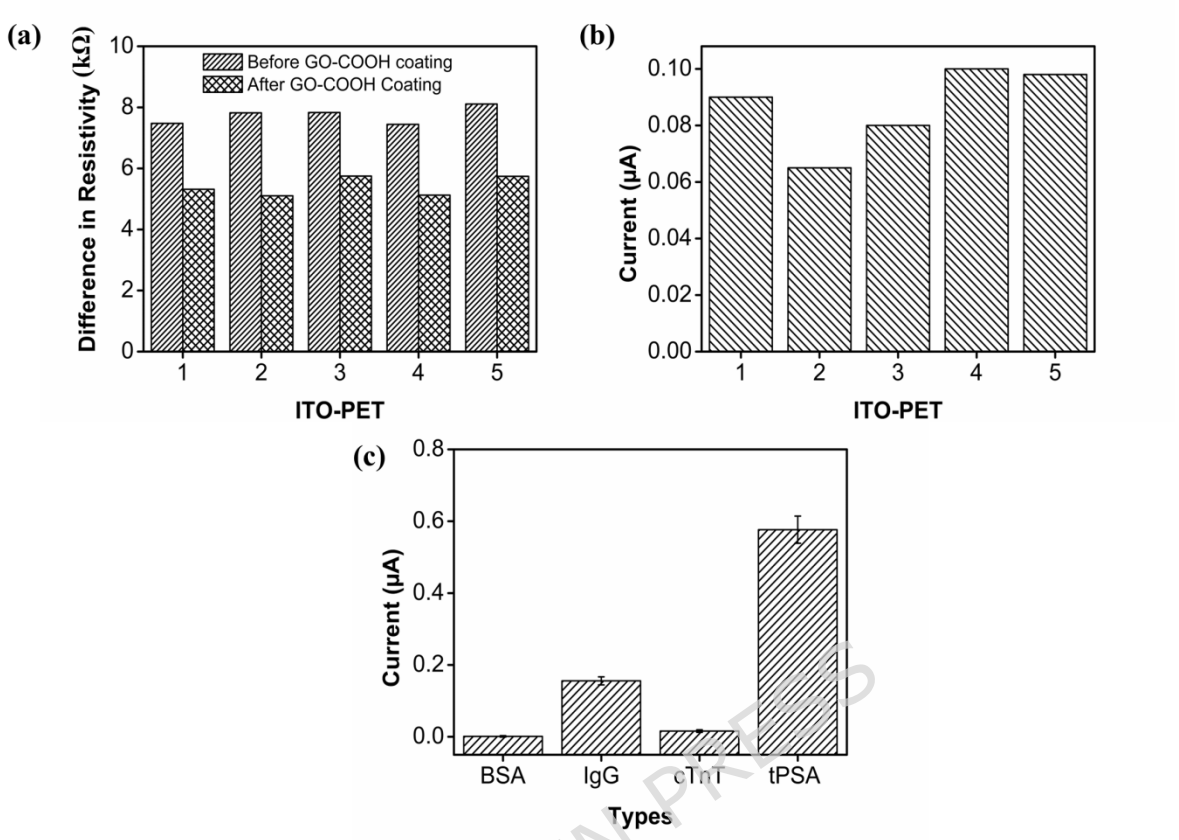

Fig. 6 (a) Comparison of charge transfer resistance (Rct) before and after GO-COOH coating on ITO-PET electrodes (n = 5). (b) Reproducibility of the GO-COOH@ITO-PET biosensor evaluated at 10 ng mL^{-1} PSA (n = 5) (c) Selectivity of the biosensor tested at 50 ng mL^{-1} PSA against potential interfering proteins (BSA, IgG, and cTnT, each at 50 ng mL^{-1}).

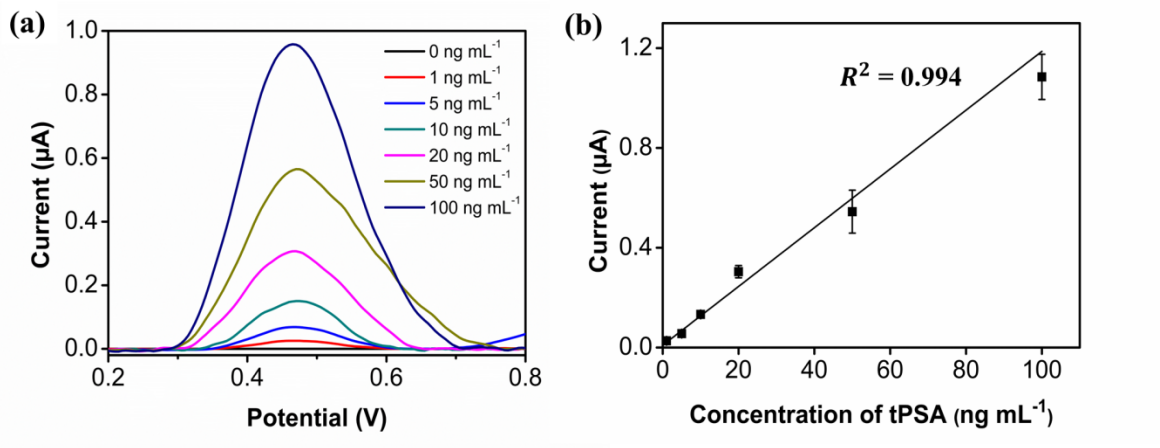

Fig. 5 (a) SWV responses of the GO-COOH@ITO-PET sensor toward PSA concentrations from 0 to 100 ng mL^{-1}, and (b) the corresponding calibration curve (SWV peak current vs. PSA).

Graphical Abstract

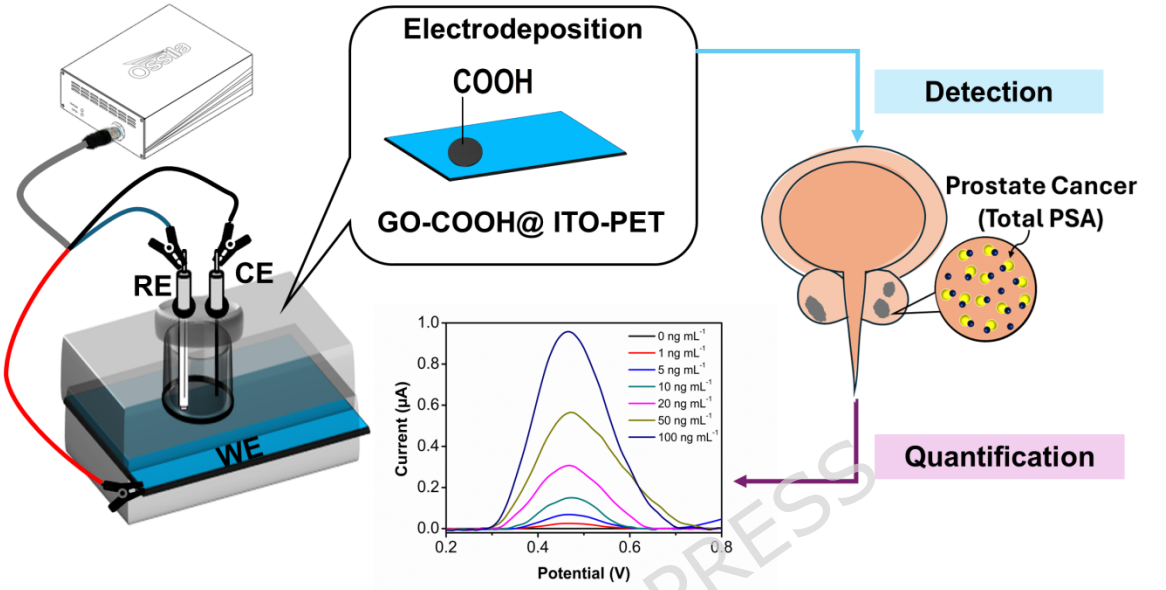

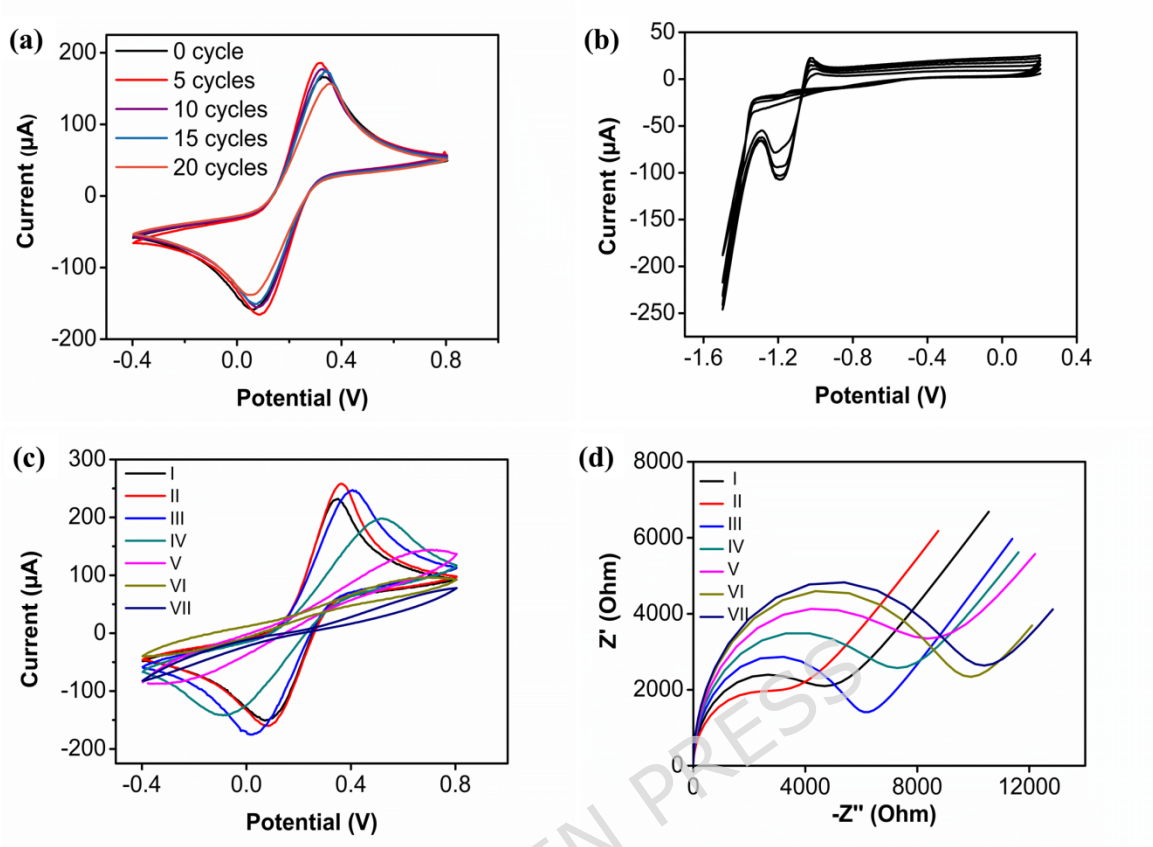

Fig. 4 (a) Electrodeposition was performed using different cycle numbers (0, 5, 10, 15, 20) at a scan rate of 50 $mVs^{-1}$with current range of 20 mA. (b) The EPD process for 5 cycles with GO-COOH on ITO-PET at potential of +0.2 V to -1.5 V(c) CV curve and (d) EIS Nyquist plot of modification stage of bare and GO-COOH coated ITO-PET. CV curves at each modification stage on ITO-PET: (I) Bare ITO-PET, (II) GO-COOH coated, (III) EDC-NHS activation, (IV) Capture antibody addition, (V) blocking reagent addition, (VI) target analyte addition, (VII) ferrocenecarboxylic acid-conjugated detection antibody addition

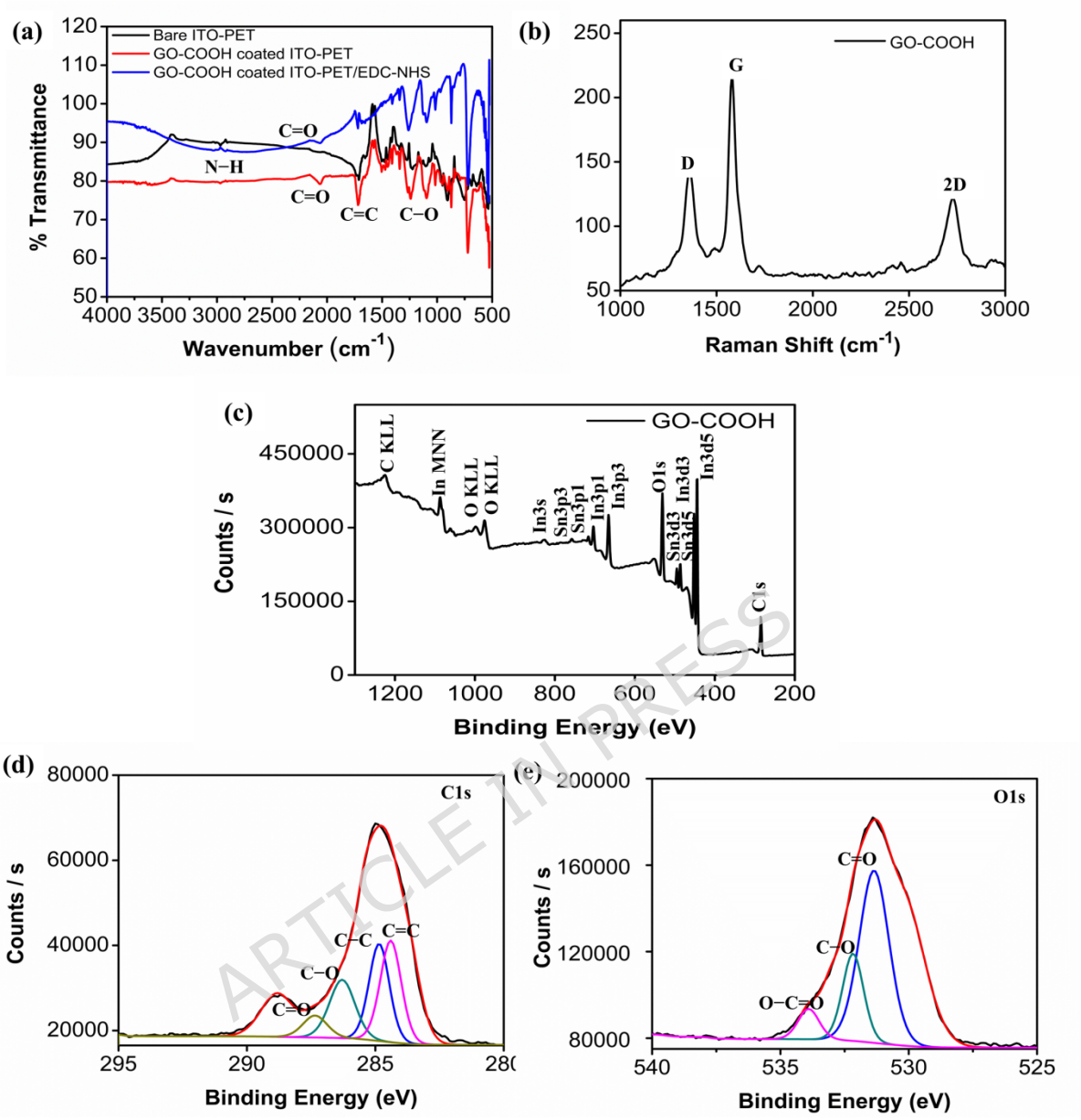

Fig. 3 (a) FTIR on surface modification on ITO-PET film with bare, GO-COOH coated and GO-COOH with EDC/NHS, (b) Raman spectra and (c) XPS survey scan of GO-COOH coated on ITO-PET and elemental profile: (i) C1s and (ii) O1s

Table 3. Comparison of PSA concentrations in clinical serum samples measured by the proposed sensor and by the CLIA method from UMMC.

Serum sample	CLIA reference (ng mL^{-1})	Proposed sensor (n=3) (ng mL^{-1})	Mean ± SD (ng mL^{-1})
1	0.53	1.5/2.3/2.7	2.2 ± 0.6
2	1.28	1.1/2.1/1.2	1.5 ± 0.5
3	3.75	3.2/3.9/2.7	3.3 ± 0.6
4	7.58	9.8/8.5/9.4	9.2 ± 0.7
5	20.99	23.8/17.9/14.7	18.8 ± 4.6
6	47.41	49.3/38.6/34.5	40.8 ± 7.6

Table 2. Recovery analysis of PSA in spiked human serum samples at different concentrations (n = 3).

Sample	Spiked Concentration (ng mL^{-1})	Measured Concentration (ng mL^{-1})	Average Recovery (%)	RSD (%)
Spiked Serum	5	6.1	128.7	5.46
		6.8		
		6.4		
	10	9.1	103.0	15.41
		12.1		
		9.7		
	50	43.1	85.4	4.06
		40.8		
		44.2		

Table 1. Comparison of representative graphene-based electrochemical immunosensors for PSA detection, emphasizing electrode substrates, immobilization strategy, and analytical performance relevant to point-of-care testing.

Electrode substrate	Detection method	Target analyte	Immobilization strategy	Linear range (ng ml $^{-1}$)	Detection limit (ng ml $^{-1}$)	Ref.
Glassy carbon electrode	[i]DPV [ii]EIS	PSA	GO/chitosan film	[i]0.1 pg mL^{-1} – 90 ng mL^{-1} [ii]5 pg mL^{-1}	[i]10 fg mL^{-1} [ii]up to 35 ng mL^{-1}	[5]
Glassy carbon electrode	EIS	DNA sequences of prostate cancer	thioglycolic acid/gold nanoparticles/reduced GO	0.0012 pg mL^{-1} – 12,000 ng mL^{-1}	0.0004 pg mL^{-1}	[12]
Glassy carbon electrode	EIS	DNA sequences of prostate cancer	polyaniline and GO nano sheets	1.0×10^{-16}M – 1.0×10^{-8} M	3.3×10^{-17} M	[11]
Screen-printed carbon	DPV	PSA	graphene-poly(3-aminobenzoic acid) nanomaterial-conductive polymer composite	0.01 ng mL^{-1} – 80 ng mL^{-1}	0.13 pg mL^{-1}	[27]
Gold substrate	DPV	PSA	reduced GO and gold nanoparticles	0.006 ng mL^{-1} – 30 ng mL^{-1}	0.003 ng mL^{-1}	[26]
Filter paper	DPV	PSA	Gold nanoparticle/reduced	0.05 ng mL^{-1}– 200 ng mL^{-1}	10 pg mL^{-1}	[29]

			GO/thionine			
Filter paper	DPV	PSA	mesoporous carbon / carbon nanotubes /GO	10.0 ng mL^{-1}–1000 ng mL^{-1}	2.16 ng mL^{-1}	[30]
ITO-PET	SWV	PSA	Carboxyl functionalized GO	0 ng mL^{-1}– 100 ng mL^{-1}	1.3 ng mL^{-1}	This work